The Chemiluminescent Cycloreversion of an Anthracene–Benzene Biplanemer System both in the Solid State and in the Liquid State

Masaru KIMURA*, Hideki OKAMOTO, and Setsuo KASHINO
Department of Chemistry, Faculty of Science, Okayama University, Tsushimanaka 3-1-1, 700
(Received February 9, 1994)

In the thermal [4+4]cycloreversions of 9-anthracenecarboxylic acid-benzene **3a**, methyl 9-anthracenecarboxylate-benzene **3b**, dimethyl (or diethyl) 9,10-anthracenedicarboxylate-benzene **3c** (or **3d**) and anthracene-1,4-difluoro(or dichloro)benzene **3f** (or **3g**) biplanemers, chemiluminescene was observed for **3a**—**d** only in the solid state at > 120 °C but not in a liquid phase, while **3f** and **3g** were not chemiluminescent. Efficient chemiluminescence was observed in the photocycloreversion of all biplanemers tested in both phases. The thermodynamic parameters for the thermal cycloreversion of these biplanemers were collected. Higher activation energies were obtained in the solid state than in the liquid phase. The higher energies favor touch of the S_0 surface with the S_1 surface at the transition state for effecting the chemiluminescent cycloreversion.

Biplanemers ([4+4]heterodimers of arenes) **3** are an energy-rich system which provides a chemiluminescent reaction and/or photochemiluminescent reaction (an adiabatic photoreaction) like Dewar arenes, dioxetanes and dioxetanones.[1] Despite a large number of photo [4+4]cycloreversions, only two examples of chemiluminescent system have been known.[2] Yang et al. and Kimura et al. have found that the chemiluminescent thermal cycloreversion of pentacyclo[6. 6. 4. $2^{15,18}$. $0^{2,7}$. $0^{9,14}$]eicosa-2, 4, 6, 9, 11, 13, 16, 19-octaene-1-carboxylic acid (9-anthracenecarboxylic acid–benzene biplanemer) **3a** and the chemiluminescent multiphoton cycloreversion of anthracene–*p*-difluorobenzene biplanemer **3f** with Nd–Yag IR laser light gave off chemiluminescent light only in the solid phase.[2a,2c] These examples suggested probability of the jump from the ground state surface (S_0) to the excited singlet state surface (S_1) in the solid phase but not in the liquid phase. As there has not been any attempt to reveal the determinants in the solid state for the chemiluminescence from thermodynamical viewpoints, this prompted us to collect the thermodynamic parameters by differential scanning calorimetry (DSC). In the case of a representative sample **3d**, two substantial exothermic processes are superimposed for the chemiluminescent crystals, whereas one main exothermic process is observed for a nonchemiluminescent powder sample. The thermodynamic parameters for the thermal cycloreversions were collected. Higher activation energy is characteristic of the chemiluminescent process prepared in the solid phase. We pointed out a possibility that the higher energy favors touch of the S_0 surface with the S_1 surface at the transition state for the effecting the chemiluminescent cycloreversion.

Results and Discussion

Synthesis and Chemiluminescent Reactions of 3. New biplanemers **3b**—**d** and known **3a**, **3f**, and **3g** were prepared by our method for biplanemers as shown in the Scheme 1.[1a,1b] The X-ray analysis of a representative chemiluminescent sample **3d** was carried out for determination of this structure. Final atomic parameters are listed in Table 1.[3] The ORTEP drawing is shown in Figure 1.[4] The bond length and angles, and selected torsion angles are listed in Table 2. Pairs of torsion angles τ_i and $\tau_{i'}$ in Table 2 have similar absolute values with opposite sign to each other except for the pair τ_{10} and $\tau_{10'}$ for the terminal bonds of the two side chains. This indicates that the main part of the molecule substantially retains the mirror symmetry also in the crystal. The elongation of the C(1)–C(12) and C(8)–C(9) bonds is remarkable. These σ bonds are nearly parallel to four adjacent π orbitals enableing a through bond coupling.[5] Another important factor for the lengthening is strong intramolecular repulsion between C(2)···C(11), 2.688(6) Å, C(7)···C(10), 2.685(6) Å, C(15)···C(13), 2.692(7) Å, and C(20)···C(14), 2.693(7) Å. The short intramolecular interactions of C=O···H–C(12 or 13) [2.23(5)—2.36(6) Å] are observed for both carbonyl groups in the molecule, which govern the conformations defined by τ_8, τ_9, $\tau_{8'}$, and $\tau_{9'}$ of the ester groups. Therefore the carbonyl group faces the long σ bond. The molecules are packed in the crystal with normal van der Waals constants. The structures of new **3b** and **3c** were assigned by comparison of the ^{1}H NMR, IR, and UV spectra with those of **3d** and the CH elemental analysis.

Benzene or acetonitrile solutions of **3a**—**d**, and **3f** were subjected to the cycloreversion reaction upon heating around 100 °C in a sealed Pyrex tube to result in nonchemiluminescent reaction, although each run gave quantitatively the corresponding anthracene **1a**—**d** and the corresponding benzene. The rates of the cycloreversion followed first-order kinetics at three temperatures in a liquid phase as listed in Table 3. The kinetic parameters determined were summarized in Table 4. When flash thermolysis of **3a**—**e** was performed in a sealed Pyrex capsule at 120 °C or 150 °C, flash light was visually detected for **3a**—**d** in the solid state and quantitative formation of **1a**—**d** was confirmed by the ^{1}H NMR analysis. When the representative case **3d** was subjected to a thermogravimetric analysis (TGA), large

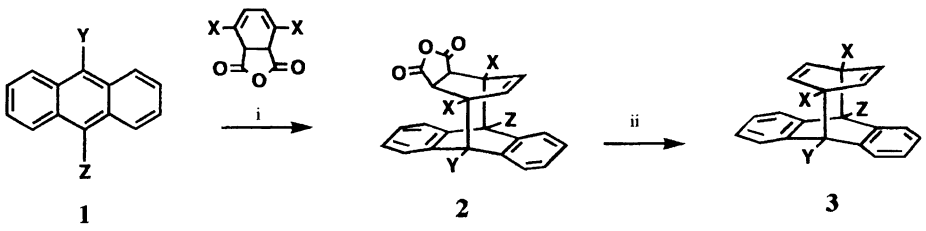

1 2 3

i) hv (pyrex) in benzene

ii) electrolysis in 80% Py aq. and TEA 2.5 eqiv./Hexane

1a: Y=COOH, Z=H
1b: Y=COOCH$_3$, Z=H
1c: Y= Z= COOCH$_3$
1d: Y= Z=COOC$_2$H$_5$
1e: Y= Z=H

2a, 3a: X=H, Y=COOH, Z=H
2b, 3b: X=H, Y=COOCH$_3$, Z=H
2c, 3c: X=H,Y= Z= COOCH$_3$
2d, 3d: X=H,Y= Z=COOC$_2$H$_5$
2e, 3e: X= Y= Z=H
2f, 3f: X=F, Y= Z=H
2g, 3g: X=Cl, Y= Z=H

Scheme 1.

Table 1. Fractional Atomic Coordinates and Equivalent Thermal Parameters B_{eq} with Their esd's in Parentheses

Atom	x	y	z	$B_{eq}^{a)}$/Å^2
C(1)	0.5834(2)	0.0763(2)	0.2880(5)	3.77(5)
C(2)	0.6039(2)	0.0959(2)	0.1387(5)	3.14(5)
C(3)	0.5824(3)	0.0716(2)	0.0142(5)	3.90(5)
C(4)	0.5980(3)	0.0917(2)	−0.1192(5)	4.72(6)
C(5)	0.6332(3)	0.1370(2)	−0.1294(5)	4.95(6)
C(6)	0.6536(3)	0.1623(2)	−0.0055(5)	4.14(5)
C(7)	0.6399(2)	0.1423(1)	0.1283(5)	3.20(5)
C(8)	0.6568(2)	0.1694(2)	0.2686(5)	3.69(5)
C(9)	0.5736(3)	0.1941(2)	0.3291(5)	4.55(6)
C(10)	0.5046(3)	0.1832(2)	0.2318(6)	4.83(6)
C(11)	0.4700(3)	0.1397(2)	0.2388(6)	4.89(6)
C(12)	0.5019(3)	0.1029(2)	0.3476(6)	4.70(6)
C(13)	0.5189(3)	0.1314(2)	0.4844(6)	5.48(7)
C(14)	0.5532(3)	0.1745(2)	0.4772(6)	5.31(7)
C(15)	0.6541(3)	0.0875(2)	0.3890(5)	3.55(5)
C(16)	0.6783(3)	0.0552(2)	0.4944(6)	4.77(6)
C(17)	0.7393(3)	0.0687(2)	0.5912(5)	5.56(7)
C(18)	0.7739(3)	0.1145(2)	0.5803(6)	5.72(7)
C(19)	0.7450(3)	0.1465(2)	0.4759(5)	4.71(6)
C(20)	0.6901(2)	0.1335(2)	0.3784(5)	3.57(5)
C(21)	0.5702(3)	0.0207(2)	0.2784(5)	4.55(6)
C(22)	0.6366(2)	−0.0012(1)	0.2337(4)	5.10(4)
C(23)	0.6373(4)	−0.0541(2)	0.2069(7)	6.81(8)
C(24)	0.6753(4)	−0.0630(2)	0.0699(8)	7.9(1)
C(25)	0.5082(2)	0.0001(2)	0.3030(5)	7.28(6)
C(26)	0.7175(3)	0.2103(2)	0.2375(6)	4.90(6)
C(27)	0.7876(2)	0.1917(1)	0.1949(4)	5.49(4)
C(28)	0.8530(4)	0.2253(2)	0.1563(10)	8.7(1)
C(29)	0.9267(4)	0.1979(3)	0.1481(9)	9.3(1)
C(30)	0.7059(2)	0.2535(1)	0.2482(6)	8.06(6)

a) $B_{eq}=(4/3)\sum_i\beta_{ii}a_i^2$.

heat evolution within 3 s was recorded at 106 °C and this was accompanied by weight loss caused by equimolar evolution of benzene as shown in Fig. 2. In the case of **3d**, the flash chemiluminescene characteristic of the

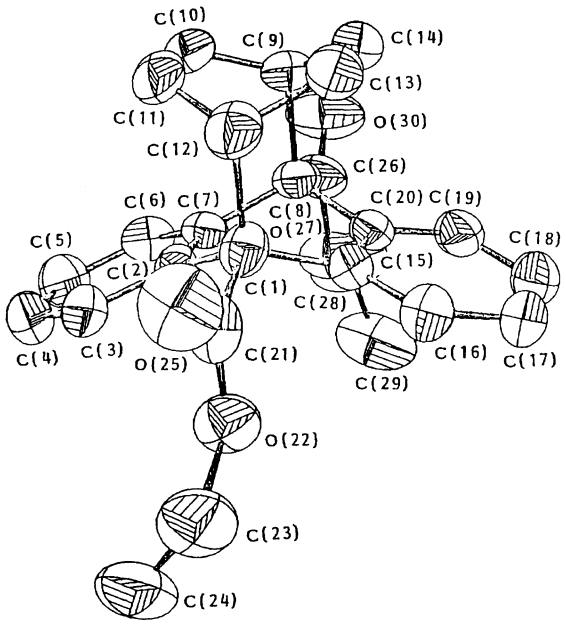

Fig. 1. The ORTEP drawing at 50% probability level of **3d** with atomic numbering. The hydrogen atoms are omitted for the sake of clarity.

fluorescence of diethyl 9,10-anthracenedicarboxylate **1d** was detected by means of a photodiode array (PMA, Hamamatsu Photonics) with a recorder of integrated light yields as shown in Fig. 3. Chemiluminescence was observed when the thermolysis was carried out by heating gradually up to the melting point or heating at 105 °C as shown in Table 5. We failed to record the dimmer chemiluminesence of **3a**—**c**. The thermolysis of **3f** and **3g** resulted in a nonchemiluminescent reaction, as in the case of **3e**, both in the solid phase and in the liquid phase.

The quantum yields (Φ_{ad}) of generation of the corresponding excited singet anthracenes in the adiabatic photoreaction of **3** were measured by the modified

Table 2. Bond Lengths (l/Å) and Angles (ϕ/°) and Selected Torsion Angles (τ/°)

C(1)–C(2)	1.529(6)	C(11)–C(12)	1.520(7)	C(2)–C(1)–C(15)	108.6(3)	C(9)–C(14)–C(13)	117.4(5)
C(1)–C(12)	1.631(6)	C(12)–C(13)	1.519(8)	C(2)–C(1)–C(21)	108.9(3)	C(1)–C(15)–C(16)	122.2(4)
C(1)–C(15)	1.535(6)	C(13)–C(14)	1.305(8)	C(15)–C(1)–C(21)	110.0(3)	C(1)–C(15)–C(20)	117.6(4)
C(1)–C(21)	1.531(6)	C(15)–C(16)	1.378(6)	C(1)–C(2)–C(3)	122.7(4)	C(16)–C(15)–C(20)	120.0(4)
C(2)–C(3)	1.383(6)	C(15)–C(20)	1.390(6)	C(1)–C(2)–C(7)	118.2(4)	C(15)–C(16)–C(17)	120.1(5)
C(2)–C(7)	1.400(6)	C(16)–C(17)	1.405(8)	C(3)–C(2)–C(7)	118.9(4)	C(16)–C(17)–C(18)	119.3(5)
C(3)–C(4)	1.383(7)	C(17)–C(18)	1.376(8)	C(2)–C(3)–C(4)	121.2(5)	C(17)–C(18)–C(19)	118.4(5)
C(4)–C(5)	1.367(7)	C(18)–C(19)	1.391(8)	C(3)–C(4)–C(5)	119.9(5)	C(18)–C(19)–C(20)	123.1(5)
C(5)–C(6)	1.387(7)	C(19)–C(20)	1.344(6)	C(4)–C(5)–C(6)	119.6(5)	C(8)–C(20)–C(15)	118.1(4)
C(6)–C(7)	1.380(6)	C(21)–O(22)	1.320(6)	C(5)–C(6)–C(7)	121.1(5)	C(8)–C(20)–C(19)	122.5(4)
C(7)–C(8)	1.527(6)	C(21)–O(25)	1.194(6)	C(2)–C(7)–C(6)	119.2(4)	C(15)–C(20)–C(19)	118.9(4)
C(8)–C(9)	1.635(7)	O(22)–C(23)	1.461(8)	C(2)–C(7)–C(8)	117.0(4)	C(1)–C(21)–O(22)	110.2(4)
C(8)–C(20)	1.519(6)	C(23)–C(24)	1.445(11)	C(6)–C(7)–C(8)	123.6(4)	C(1)–C(21)–O(25)	125.2(5)
C(8)–C(26)	1.529(8)	C(26)–O(27)	1.329(7)	C(7)–C(8)–C(20)	109.5(4)	O(22)–C(21)–O(25)	124.6(5)
C(9)–C(10)	1.490(7)	C(26)–O(30)	1.195(8)	C(7)–C(8)–C(26)	108.1(4)	C(21)–O(22)–C(23)	120.4(5)
C(9)–C(14)	1.518(8)	O(27)–C(28)	1.464(10)	C(20)–C(8)–C(26)	110.9(4)	O(22)–C(23)–C(24)	108.7(6)
C(10)–C(11)	1.317(7)	C(28)–C(29)	1.434(13)	C(10)–C(9)–C(14)	108.2(4)	C(8)–C(26)–O(27)	110.8(5)
				C(9)–C(10)–C(11)	118.9(5)	C(8)–C(26)–O(30)	126.5(6)
				C(10)–C(11)–C(12)	118.2(5)	O(27)–C(26)–O(30)	122.7(6)
				C(11)–C(12)–C(13)	106.8(4)	C(26)–O(27)–C(28)	119.0(5)
				C(12)–C(13)–C(14)	119.8(5)	O(27)–C(28)–C(29)	108.7(7)

τ_1 C(12)–C(1)–C(2)–C(3)	−97.3(5)	$\tau_{1'}$ C(9)–O(8)–C(7)–C(6)	97.4(5)
τ_2 C(15)–C(1)–C(2)–C(3)	142.7(4)	$\tau_{2'}$ C(20)–C(8)–C(7)–C(6)	−142.0(4)
τ_3 C(2)–C(1)–C(12)–C(11)	−0.4(5)	$\tau_{3'}$ C(7)–C(8)–C(9)–C(10)	0.3(5)
τ_4 C(15)–C(1)–C(12)–C(11)	118.9(4)	$\tau_{4'}$ C(20)–C(8)–C(9)–C(10)	−120.1(4)
τ_5 C(15)–C(1)–C(12)–C(13)	0.5(5)	$\tau_{5'}$ C(20)–C(8)–C(9)–C(14)	0.2(6)
τ_6 C(21)–C(1)–C(12)–C(11)	−120.2(4)	$\tau_{6'}$ C(26)–C(8)–C(9)–C(10)	118.4(5)
τ_7 C(12)–C(1)–C(15)–C(16)	97.4(5)	$\tau_{7'}$ C(9)–C(8)–C(20)–C(19)	−93.6(5)
τ_8 C(12)–C(1)–C(21)–O(25)	3.9(7)	$\tau_{8'}$ C(9)–C(8)–C(26)–O(30)	−3.4(8)
τ_9 C(23)–O(22)–C(21)–O(25)	1.7(8)	$\tau_{9'}$ C(28)–O(27)–C(26)–C(30)	−1.4(9)
τ_{10} C(21)–O(22)–C(23)–C(24)	133.0(6)	$\tau_{10'}$ C(26)–O(27)–C(28)–C(29)	166.2(6)

method of Berlman using the emission of nonchemiluminescent **3f** as a standard both in the liquid phase and in the solid state because the efficiency for **3f** is almost quantitative ($\Phi_{ad}>0.99$) in hexane.[6,16] The photocycloreversion of **3a**—**d** adiabatically provided the corresponding anthracene in the singlet excited state in less efficiency than those of **3e** and **3f** both in the solid state and in the liquid phase. Further the relative efficiency for the adiabatic photoreaction of **3a**—**d** in the solid state is commonly smaller than those in the liquid phase as summarized in Table 6.

Determination of Heats and Kinetic Parameters of the Cycloreversions in the Solid state by Differential Scanning Calorimetry (DSC). The thermograms of **3a**—**d** are shown in Fig. 4, which were obtained by using samples of about the same weight (2 mg) and increasing the temperatures from ca. 80 to ca. 180 °C. The heats (ΔH) for the thermolysis in the solid state were measured by linearly increasing temperature using DSC at three heating rates (β) in order to extract the thermodynamic parameters. The exotherm of the cycloreversion calculated from DSC thermograms was analyzed with the usual Eq. 1 for the kinetics the cycloreversion of solids:

$$d\alpha/dt = \beta d\alpha/dT = A \exp(-E_a/RT)(1-\alpha)^n, \quad (1)$$

where α is the fraction of decomposition and E_a is activation energy. $d\alpha/dt$ denotes the rate of decomposition and equals to $k(1-\alpha)^n$ for the nth ordered reaction with the rate constant k. Their activation parameters were determined by the difference-differential method of Freeman and Carroll followed by Friedman plots of ΔH in the temperature range from 95 to 150 °C.[7a,7b] The biplanemers undergo the [4+4]cycloreversion below the melting point of the corresponding anthracenes to give the pure solid mass of the product anthracenes. From thermograms, first-order kinetics are found for **3a**, **3b**, and **3d** but not for **3c** and **3f**. In the case of **3c** and **3f**, only the ΔH was listed because uncharacterized endothermic changes were superimposed as shown in Fig. 4. In the case of **3d**, it is remarkable that two exothermic changes are superimposed as shown in Fig. 4 (d)-1. Donati et al. described a similar exothermic change in the monomerization of the 9-cyanoanthracene dimer, the thermogram of which shows peaks superimposed on a broad exothermal peak associated with the dimer to monomer reaction.[8] They pointed out that the first peak is sample dependent and ascribable to the cycloreversion accompanied by the structural change of the crystal. The first peak located in the lower temperature range for **3d** is also ascribable to the cycloreversion accompanied by the structural change of

Table 3. First Order Rate Constants for the Thermal Cycloreversion of **3** in a Liquid Phase

Compd	Solvent	Temp/°C	k/s^{-1}
3a	Xylene	42	7.53×10^{-5}
		54.5	5.07×10^{-4}
		65	1.37×10^{-3}
	DMF	43	3.13×10^{-5}
		59	2.67×10^{-4}
		70	1.85×10^{-4}
3g	Xylene	26	5.20×10^{-5}
		32	1.01×10^{-4}
		38	2.28×10^{-4}
		41	3.69×10^{-4}
		46	6.28×10^{-4}
		52	1.35×10^{-3}
		61	3.57×10^{-3}
	MeCN	26	1.52×10^{-5}
		33	4.24×10^{-5}
		39	8.38×10^{-5}
		53	7.00×10^{-4}
		61	1.46×10^{-3}
		65	2.89×10^{-3}
3d	Xylene	32	7.44×10^{-5}
		47	5.37×10^{-4}
		60	3.19×10^{-3}
	MeCN	35.5	35.5×10^{-5}
		47	2.57×10^{-4}
		59.5	1.33×10^{-3}
3f	Xylene	81	1.73×10^{-5}
		94	6.35×10^{-5}
		110	3.72×10^{-4}
3g	Xylene	42	8.46×10^{-6}
		63	1.42×10^{-4}
		71	2.89×10^{-4}

Table 4. Activation Parameteres for the Thermal Cycloreverson of **3**

Compound	Phase	$\Delta H^{\neq}$	$\Delta S^{\neq}$	ΔH
		kcal mol^{-1}	eu	(kcal mol^{-1})[a]
3a	Solid	25.8	10.0	26.3
	in DMF	25.2	0.87	
	in Xylene	27.0	8.4	
3b	Solid Lα[b]	36.8	74.0	17.2
	Hα[b]	27.3	46.0	
3c	Solid	—	—	23.0
	in MeCN	26.4	7.2	
	in Xylene	23.8	1.4	
3d	Solid LT[c]	28.8	10.0	25.8
	HT[c]	25.8	0.8	
	in MeCN	26.6	7.2	
3e[d]	MeOH	33.0	16.4	
3f	Solid	—	—	16.3
	in Xylene	27.4	−0.64	
3g	in Xylene	26.8	3.5	

a) Detrmined by DSC analysis; b) Lα: Lower conversion region; Hα: Higher conversion region shown in Figure 6; c) LT: Lower temperature region of DSC curve; HT: Highr temperature region of DSC curve; d) Ref. 2c.

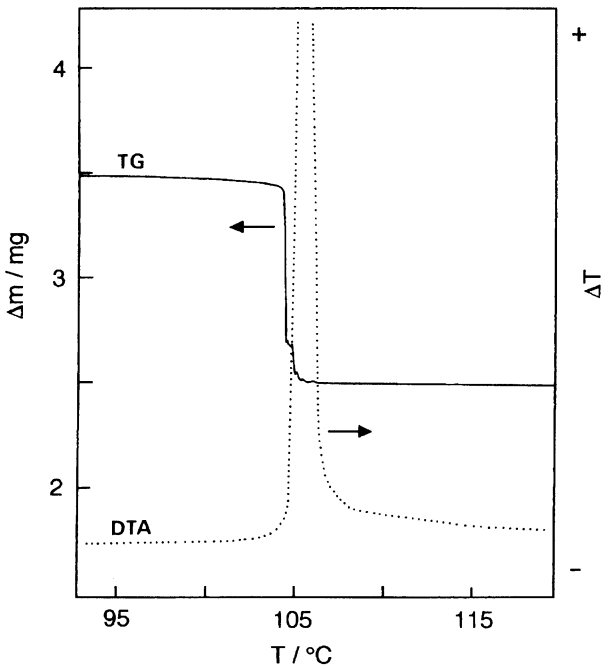

Fig. 2. The Thermogravimetric Analysis (TG) and the Differential Thermal Analysis (DTA) of the Cycloreversion of **3d**; Sample weight=8.3 mg and Scan Speed=5°C min^{1}.

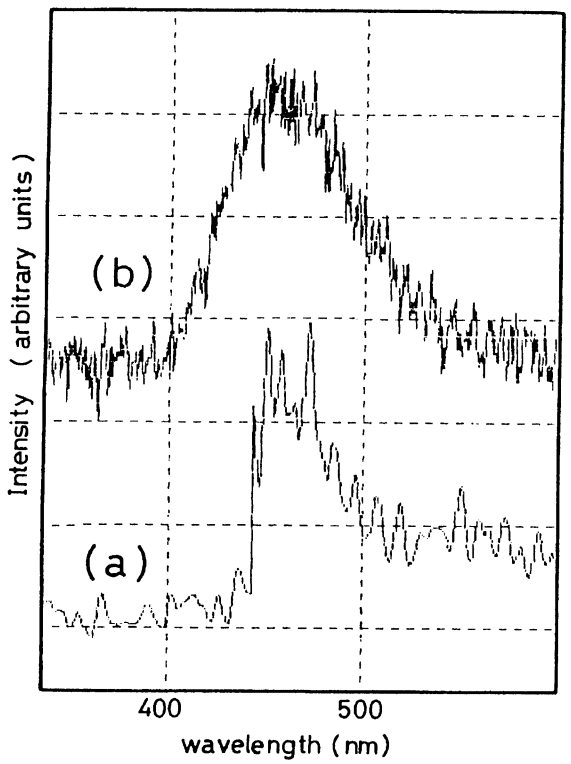

Fig. 3. (a) Chemiluminescence spectrum of **3d** at 150 °C and (b) the Fluorescence Spectrum of **1d** at 25 °C in the Solid Phase.

Table 5. Observation of the Chemiluminescence of Crystalline **3d** under Various Conditions

Conditons		Chemiluminescent (CL) or Dark reaction (D)
Form	Temp/°	
Crystals[a)]	150	CL
Crystals[a)]	120	CL
Crystals[a)]	105	D
Grinded crystals	150	CL
Annealed crystals at 105 °	150	D
Powder	150	D

(a) Crystal Size: 1.5 —0.5mm×0.4—0.025 mm.

the crystal because the first one is also sample dependent. When the powder of **3d**, obtained by evaporation of the solvent of a dichloromethane solution by a rotary evaporator, was subjected to the flash thermolysis at 150 °C, chemiluminescence was not observed visually. Grinding the chemiluminescent crystals into powder has no effect on the chemiluminescence, whereas annealing the crystals at 105 °C changed to nonchemiluminescent one (Table 5). It is notable that (a) the sample possessing the large peak at lower temperature range relates to chemiluminescent reaction, while (b) the sample possessing only one peak at higher temperature range is not a chemiluminescent one. Although we intended to investigate a solid structure of the nonchemiluminescent powder, we failed to grow a sufficient size of nonchemiluminescent for X-ray analysis. Although in the case of **3a** and **3b** there is one broad exothermic peak, two cycloreversion processes were revealed by the plot of the activation energies vs. α. The activation parameters for the cycloreversion of **3a**, **3b**, and **3d** in the solid phase are summarized in Table 4. The activation energies increase in the order of **3d**>**3a**>**3b** in parallel to the order of their chemiluminescence intensities confirmed visually. The cycloreversion of **3d**(d-1) in the higher temperature range seems to show an amorphous nature of nonchemiluminescent powder (d-2), and the kinetic parameters in this range are substantially the same as those in the xylene where the molecules are free from the arrangement in the chemiluminescent crystals.

Two different sets of kinetic parameters of **3b** were collected from the α range from 0.0—0.5 and the range 0.5—1.0. The activation energies were estimated to be 154.8 kJ mol^{-1} and 104.6 kJ mol^{-1}, respectively. Two sets of kinetic parameters of **3d** were also collected from the both peaks and the activation energies for the low temperature range and for the high temperature range are 121.3 kJ mol^{-1} and 106.3 kJ mol^{-1}, respectively. Judging from the observation made for **3b** and **3d**, the higher activation energy probably arises from releasing stain during structual change in the chemiluminescent crystals, while the lower activation energy probably reflects looseness in an amorphous phase. How do these efficiency profiles correlate to chemiluminescence only in the solid state. Discussed on the bases of correlation diagrams such as those depicted in Fig. 5 will help to rationalize the difference in cycloreversion manner in the different media.[2a,6,18)]

Energy Surface Diagram for the Reactions of 3. Figure 5 is energy surface diagram for the reactions of **3** based on the conservation of orbital symmetry including consideration of electronic and thermodynamic data collected in the present work.[6,18)] The ground state energy of **3** (BP_0) is set to 240.6 kJ mol^{-1} by adopting Yang's estimating for **3e**.[2c)] Triplet and singlet excited state of **3** are set 292.9 kJ mol^{-1} and 460.2 kJ mol^{-1} of the benzene moiety (B).[1b)] Triplet and singlet excited states of products are set for anthracene 128.9 kJ mol^{-1} and 167.4 kJ mol^{-1}, respectively. The doubly excited state of products $(An+B)^{**}$ is estimated as the sum of the triplet energies of An (anthracene, 179.1 kJ mol^{-1})[17a)] and B. $^1BP^*$–$^1An^*$ correlation line provides S_1 surface based on the Michl proposal.[18a)] Doubly excited state of **3** (BP^{**}) are estimate as the sum of the triplet energies of ethylene (343.1 kJ mol^{-1})[17b)] and B. As the $BP_0-(An+B)^{**}$ and $BP^{**}-(An+B)$ line crossing is avoided, ground state S_0 [$BP_0-(An+B)$ line] and doubly excited D [$BP^{**}-(An+B)^{**}$ line] surfaces are provided. As shown in Table 6 very efficient anthracene fluorescence was observed as a result of the adiabatic photoreaction of **3** in hexane. Even in the solid state, the efficiency of the adiabatic photoreaction is relatively high as the result of fundamental crossing between the S_1 surface and the doubly excited surface.

For the thermal cycloreversion, higher activation energies were obtained in the solid state than in the liquid phase and then it implies touch of the S_0 surface with the S_1 surface at the transition state in the solid state as shown in Fig. 5. Thus in the case of **3a**—**d**, a more efficient partitioning channel from the S_0 surface into the S_1 surface is prepared in the solid state reaction than that in the liquid phase. We can point out another advantage in the solid state to generate the excited molecules. In comparison of the emission spectra (Fig. 6) and the excitation spectra (Table 7) observed in the adiabatic photoreaction of **3a**—**d** in the liquid phase with those in solid state, a shift toward a longer wavelength side by about 5 nm was clear both for excitation peaks around 385 nm and for photochemiluminescences at λ_{min}. These shifts make the energy gap between S_0 and S_1 surfaces shallower in the solid state than in the liquid phase because ΔE_{ex} and ΔE_{em} are positive (Table 7). Therefore in the solid phase, preferable conditions for chemiluminescence are prepared both in the transition state and over the excited singlet surface.

Experimental

Apparatus and General Procedures. Melting points were measured with a Yanagimoto micro melting point apparatus and were uncorrected. ^1H NMR spectra were recorded on a JEOL JNM PMX-60 spectrometer or

Table 6. The Emission Quantum Yields (Φ_E) of Anthracenes **1** and Biplanemers **3**, Efficiencies (Φ_{ad})[b] of Generation of $^1\mathbf{1}^*$ in the Adiabatic Photoreaction of **3** in a Liquid Phase

Compd	Solvent	Φ_E	Φ_{ad} Liquid phase	Relative efficiency Solid phase[c]
1a	CH_2Cl_2	0.24		
1b	Hexane	0.63		
	CH_3CN	0.30		
1c	Hexane	0.70		
	CH_3CN	0.69		
1d	CH_2Cl_2	0.75		
1e	Hexane	0.30 (0.30[a])		
	CH_3CN	0.24		
3a	CH_2Cl_2	0.17	0.72	0.31
3b	Hexane	0.50	0.79	0.58
	CH_3CN	0.21	0.69	
3c	Hexane	0.60	0.86	0.35
	CH_3CN	0.45	0.65	
3d	Hexane	0.54	0.72	0.46
3e[d]	Hexane	0.19	0.80	
3f	Hexane	0.30	1.0[e]	1.0
3g	Hexane	0.13	0.43	
	CH_3CN	0.33		

a) Fluourescence Quantum Yields of Anthracencenes (Φ_f) are cited from Ref. 2f; b) Efficiencies of Generation of Anthracenes in the Excited Single state in Adiabatic Photoreaction of Biplanemers [$\Phi_{ad}=\{\Phi_f$ of **3**$\}/\{\Phi_f$ of **1**$\}$] in a Liquid Phase; c) Relative efficiency$=\{\Phi_f$ of **3**$\}/\{\Phi_f$ of **3f**$\}$; d) Ref. 2c. e) Ref. 2g.

Varian XL-500 in $CDCl_3$. IR spectra were recorded on a JASCO FT-IR 5000 spectrometer. UV spectra were recorded on a Hitachi 228 spectrophotometer. Fluorescence spectra were recorded on a Hitachi PF-4 spectrophotometer. Elemental analyses were performed on a Yanaco MT-2 CHN-corder. All solvents used for measurements of absorption and emission spectra were purified by conventional procedures. Biplanemers **3f** and **3g** were prepared by our method.[2a] *trans*-1,2-Dihydrophthalic acid was prepared by the method of McDonald and Reineke.[9]

Kinetics of the Cycloreversion of Biplanemers. (a) In Liquid Phases: For first-order reaction the rate constant was obtained at definite temperature by supposing that a mol of reactant is initially present in unit volume of the reacting system and x mol in unit volume has reacted after time t. The ratio $a(a-x)^{-1}$ was determined by the measurement of UV absorption spectra of the solution at $\lambda=365$ nm for the generating anthracene. The representative UV spectral change for a sample of **3d** was obtained as follows: a 2 mg sample was dissolved in CH_3CN. An aliquot (5 cm^3) was transferred into a Pyrex reaction tube and the sample tube was shielded. After the reaction was performed in a constant temperature bath it was stopped by chilling the sample, the UV absorption spectra of the solution was taken at appropriate time intervals until 50% conversion. The data for **3a**—**c**, **3f**, and **3g** are also collected and Arrhenius plots were carried out for each case.[10] All activation parameters obtained are summarized in Table 4.

(b) In the Solid Phase: Thermograms of the compounds studied were obtained by means of a Perkin–Elmer or Shimadzu Differential Scanning Calorimeter Mod. DSC-7 including a data analyzer and plotter. Samples were sealed in the usual aluminium volatile sample pans; an empty pan was used as reference. Both the sample and reference holders were covered with aluminium holder covers. For **3a**—**d**, and **3f** the conditions used were: Range (R) 1 mcal s^{-1} full scale and scan speed (SS)$=\beta=dT/dt=1,2$, and 3 °C min^{-1}. Ea was obtained from the slope of the Friedman plots of $\ln(\beta d\alpha/dT)=\ln A(1-\alpha)^n-E_a/RT$. The factor A and n were obtained from the plot of $\ln A(1-\alpha)^n=\ln A+n\ln(1-\alpha)$.

Values of n for **3a**, **3b**, and **3d** were 0.8, 0.9, and 0.95 respectively.

Crystal Structure Analysis of 3d. chemiluminescent crystals of **3d** were grown by slow addition of ethanol into a solution containing a minimum amount of methylenechloride. A crystal with the dimensions 0.35×0.35×0.30 nm was mounted on a glass fiber. Diffraction measurements were made on a Rigaku AFC-5R diffractometer with graphite monochromated Mo $K\alpha$ radiation ($\lambda=0.71073$ Å, 40 kv, 200 mA) at the X-Ray Laboratory of Okayama University. Cell constants were determined from a least-squares refinement using 25 reflections in the 2θ range of 21° to 23°.

Crystal data: $C_{26}H_{24}O_4$, $M_r=400.47$, orthorhombic, *Pnca* (No. 60), $a=16.588(8)$, $b=27.21(1)$, $c=9.323(4)$ Å, $V=4209(3)$ Å^3, $D_x=1.264$ Mg m^{-3}, μ(Mo $K\alpha$)$=0.091$ mm^{-1}, $F(000)=1696$.

The intensity data were collected at 298 K using the ω–2θ scan method to a maximum 2θ of 50° [scan width $(0.89+0.30\tan\theta)$° in ω, scan speed 6° min^{-1} in ω]. Of 4317 reflections ranging $h=0$ to 19, $k=0$ to 32, $l=-1$ to 11, 3119 were unique ($R_{int}=0.018$). The fluctuations of the intensities of three standard reflections, which were measured after every 97 reflections, were within 1.4%. The data were corrected for Lorentz and polarization effects. An absorption correction was not applied. The structure was solved by the direct method (MULTAN84).[11] The non-H atoms were refined

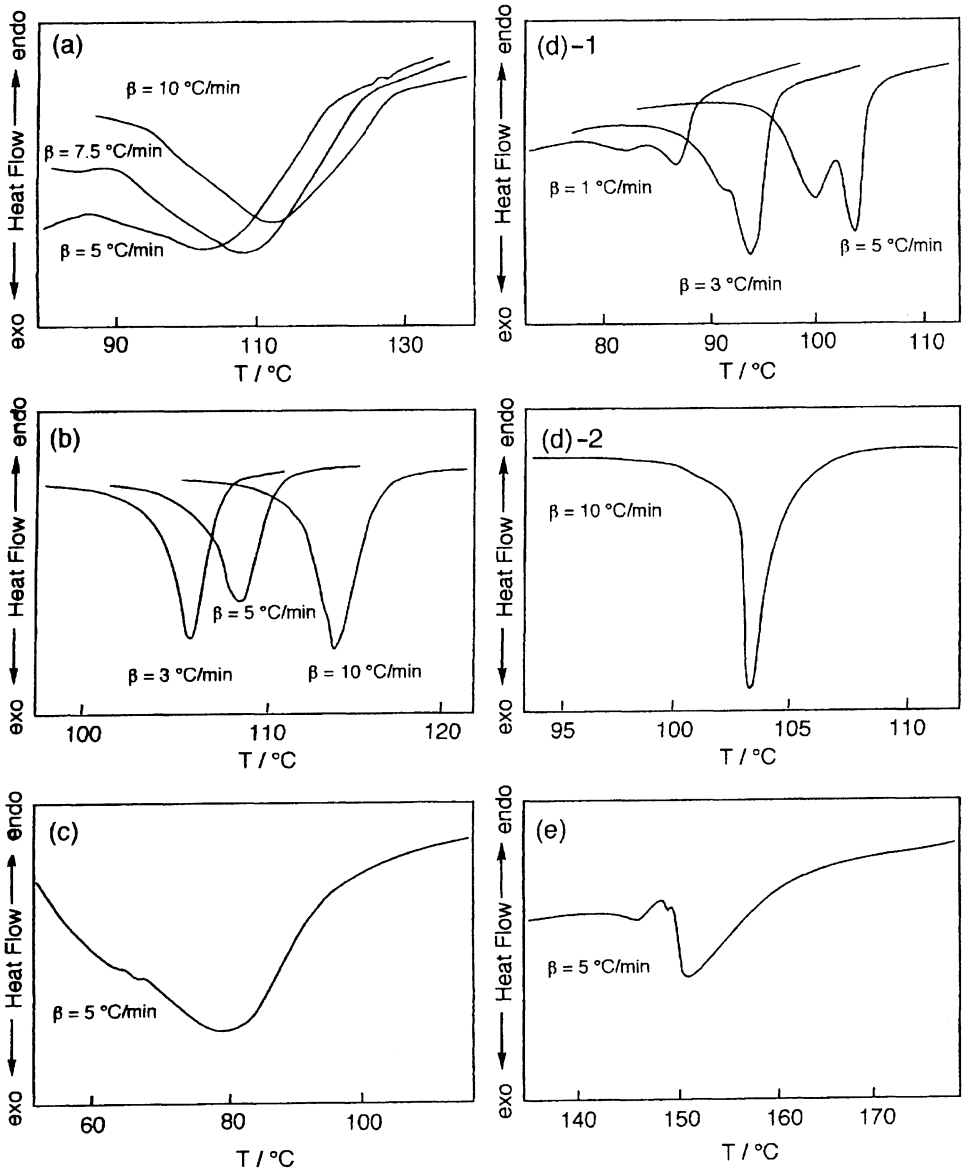

Fig. 4. Diagrams of exothermic changes for the thermolysis of **3a**—**e** in the solid state at heating rates (b); (a) **3a**, (b) **3b**, (c)**3c**, (d-1) chemiluminescent crystal **3d**, (d-2) powder **3d**, and (e) **3f**.

anistropically by block-diagonal least- squares methods.[12] The H-atoms were found in a difference Fourier map, and were refined isotropically. The final cycle of least-squares was based on 2146 reflections with $|F_o|$ larger than $3\sigma(F_o)$ and 368 variable parameters. $\sum w(|F_o|-|F_c|)^2$ was minimized with $w=[\sigma^2(F_o)+0.1006|F_o|-0.0001|F_o|^2]^{-1}$. Final $R=0.071$, $wR=0.082$, and $S=1.15$.$(\Delta/\sigma)_{max}$ was 0.37. The maximum and minimum $\Delta\rho$ in the final difference Fourier map were 0.3 and -0.3 e Å^{-3}.

The atomic scattering factors were taken from International Tables for X-Ray Crstallography.[13] Calculations were performed at the Okayama University Computer Center.

Photoadduct 2c. *trans*-1,2-Dihydrophthalic acid(1.5 g, 8.0 mmol) was converted to *cis*-anhydride by treatment with Ac_2O under reduced pressure;[9] residual *cis*-1,2-dihydrophthalic anhydride was used following photoreaction without further purification. The *cis*-anhydride and dimethyl anthracene-9,10-dicarboxylate (0.5 g, 1.7 mmol) were dissolved in 230 cm^3 of benzene. The solution was irradiated with a 100 W high-pressure Hg lamp through a Pyrex filter for 24 h under a nitrogen atmosphere. After concerning of the solution, the residue was passed through a silica-gel column using CH_2Cl_2 as an eluent to give the photoadduct **2c** (0.62 g, 1.4 mmol, 83 %) which was recrystallized from CH_2Cl_2–EtOH to give colorless crystals; mp 245—247 °C; ^{1}H NMR (60 MHz) δ=6.75—7.37 (m, 8H, ArH), 5.55 (m, 2H), 3.89 (s, 6H), and 2.80 (bs, 2H); IR (KBr) ν_{max} 1847, 1781, and 1734 cm^{-1}; UV (EtOH) λ_{max} 271 ($\log\varepsilon$=2.45), and 278 nm (2.45). Found: C, 70.19; H, 4.30%. Calcd for $C_{26}H_{20}O_7$: C, 70.27; H, 4.54%.

Photoadduct 2b. Compound **2b** was prepared by the method of **2c** from *cis*-1,2-dithydrophthalic anhydride and methyl anthracene-9-carboxylate in 92% yields as colorless needles; mp 251—253 °C; ^{1}H NMR (60 MHz) δ=6.67—7.26 (m, 8H, ArH), 5.53 (m, 2H), 4.57 (m, 1H), 4.38(d, 2H, J= 10 Hz), 3.95 (s, 3H), 3.67 (m, 1H), and 2.97 (bs, 2H); IR

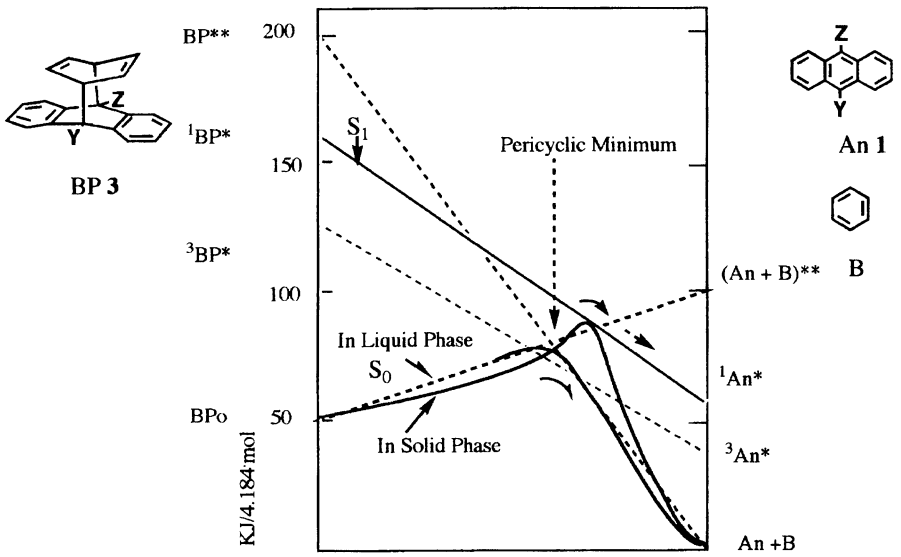

Fig. 5. The energy surface diagram for the reactions of biplanemer **3** based on the conservation of orbital symmetry.[18] An=anthracene, B=Benzene.

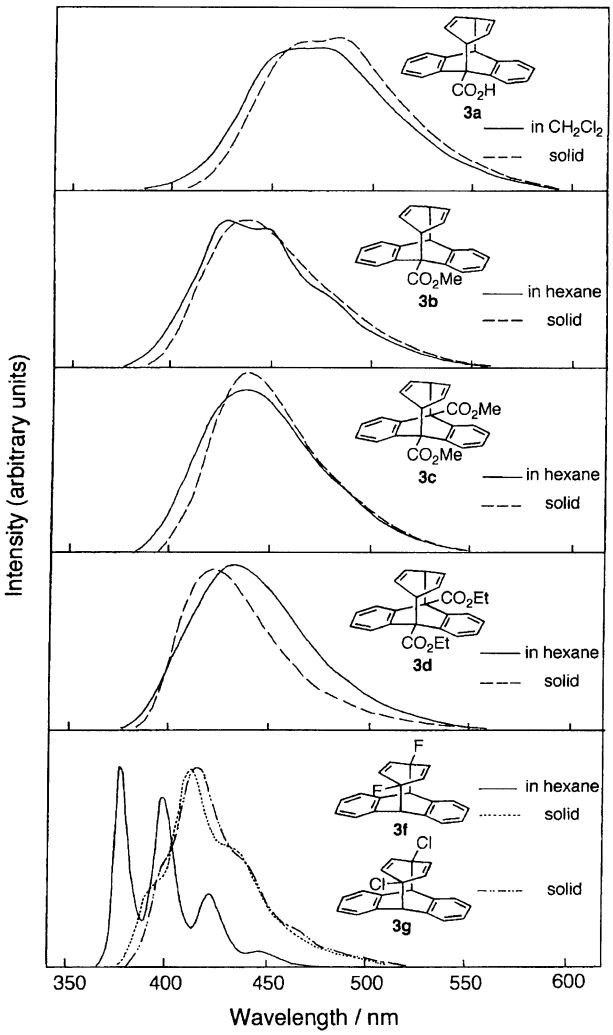

Fig. 6. Comparison of emission spectra of **3a**—**g**.

(KBr) ν_{max} 1834, 1762 and 1722 cm^{-1}; UV (EtOH) λ_{max} 270 ($\log\varepsilon$=2.82), and 278 nm (2.86). Found: C, 74.60; H, 4.62%. Calcd for $C_{24}H_{18}O_5$: C, 74.60; H, 4.70%.

Photoadduct 2d. Compound **2d** was prepared by the method of **2c** from *cis*-1,2-dihydrophthalic anhydride and diethyl anthracene-9,10-dicarboxylate in 70% yield as colorless needles; mp 223—225 °C; ^{1}H NMR (60 MHz) δ=6.73—7.40 (m,8H, ArH), 5.54 (m, 2H), 4.63 (m, 2H), 4.43(q, 4H, J=6.4 Hz), 2.79 (bs, 2H) and 1.32 (t 3H, J=6.4 Hz); IR (KBr) ν_{max} 1854, 1781, and 1734 cm^{-1}; UV (EtOH) λ_{max} 270 ($\log\varepsilon$=2.74), and 278 nm (2.68). Found: C, 71.01; H, 5.06%. Calcd for $C_{28}H_{24}O_7$: C, 71.18; H, 5.12%.

Biplanemer 3c. An icecooled mixture of **2c** (300 mg, 0.68 mmol), 4-*t*-butylcatechol[14] (18 cm^3) and silica gel (ca. 20 mg) in 25 cm^3 of a mixed solvent (MeCN : pyridine : water : triethylamine=18 : 5 : 2 : 1 in volume) was electrolyzed using a pair of platinum plate electrodes with a current of 150 mA for 4h. After filtration of silica gel, the filtrate was concentrated under reduced pressure to ca. 5 cm^3. The residual brown tar was extracted with ether (50 ml). The extract was washed with 2 M HCl (1 M=1 mol dm^{-3}) and then with ice-water twice. The ethereal solution was dried over anhyd. $MgSO_4$ and ether was evaporated under reduced pressure. The residue was chromatographed using TLC (silica gel, CH_2Cl_2 : hexane=1 : 1) and a fraction containing **3c** (R_f=0.5—0.6) was collected. Recrystallization from $CHCl_3$–EtOH gave colorless needles (40 mg, 0.11 mmol, 16%); mp 178—178.5 °C ^{1}H NMR (500 MHz) δ=6.63—7.23 (m, 8H), 5.70 (m, 4H), 4.32 (m, 2H), and 3.87 (s, 6H); IR (KBr) ν_{max} 1727, 1472 and 1431 cm^{-1}; UV (EtOH) λ_{max} 276 ($\log\varepsilon$=3.12), and 284 nm (3.19). Found: C, 77.30; H, 5.42%. Calcd for $C_{24}H_{20}O_4$: C, 77.40; H, 5.41%.

Biplanemer 3a. Compound **3a** was prepared by hydrolysis of **3b** using the method of Gassman and Shenk[15] in 78 % yield as colorless crystals; mp 95 °C (decomp); ^{1}H NMR (500 MHz) δ=7.20 (bs, 1H), 7.14 (m, 8H), 5.86 (m, 4H), 4.39 (m,2H), 4.44 (m,1H), 4.37 (d, 1H, J=10.5 Hz), 3.47 (m, 1H) and 3.37 (m, 1H); IR (KBr) ν_{max} 3280—

Table 7. Photochemiluminescence and Excitation spectra Data of the Adiabatic Photoreaction of **3** Both in the Solid and Liquid Phase

Compd	Solvent or State	Emission[a] λ_{min}/nm	ΔE_{em}[c] kJ mol^{-1}	Excitation[b] λ_{man}/nm	ΔE_{ex}[c] kJ mol^{-1}
3a	CH_2Cl_2	413		285	
	Crystal	417	7.1	288	4.6
3b	Hexane	368		285	
	Crystal	397	6.7	301	22.2
3c	Hexane	393		284	
	Crystal	403	3.3	291	8.8
3d	Hexane	385		284	
	Crystal	391	4.6	290	10.0
3f	Hexane	366		282	
	Crystal	379	11.3	291	13.0
3g	Hexane	368		284	
	Crystal	385	10.9	280	−6.3

a) Determined from uncorrected spectra; b) Values obtained by extapolating the straight portion of the high energy side of the chemiluminescence curve to zero intensity; c) The excitation energy gap between liquid phase and solid state (ΔE_{ex}) and chemiluminescence energ gap estimated from the high energy side between liquid phase and solid state (ΔE_{em}).

2720, and 1745 cm^{-1}; UV (MeCN) Λ_{max} 277 ($\log\varepsilon$=3.11), and 285 nm (3.27). Found: C, 75.80; H, 5.57%. Calcd for $C_{21}H_{16}O_2 \cdot 1.8H_2O$: C, 75.80; H, 5.89%. Compound **3a** had been reported by N. C. Yang and X. Yang, but its elemental analysis and its spectral data were not known.[2e]

Biplanemer 3b. Compound **3b** was prepared by the similar method for **3c** in 10% yield as colorless needles; mp 108—109 °C; ^{1}H NMR (60 MHz) δ=6.60—7.17 (m,8H, ArH), 5.77 (m, 4H), 4.37(m, 2H), 4.27 (d, 2H, J=13 Hz) and 3.47 (m, 1H); IR(KBr) ν_{max} 1718, and 1465 cm^{-1}; UV (EtOH) λ_{max} 276 ($\log\varepsilon$=3.20), and 285 nm (3.35). Found: C, 83.45; H, 5.59%. Calcd for $C_{22}H_{18}O_2$: C, 84.05; H, 5.77%.

Biplanemer 3d. Compound **3d** was prepared by the method of **3c** in 16% yield as colorless needles; mp 171—172 °C; ^{1}H NMR (60 MHz) δ=6.63—7.37 (m, 8H), 5.70 (m, 4H), 4.30 (m, 2H), 4.39 (q, 4H, J=6.4 Hz), and 1.30 (t, 6H, J=6.4 Hz); IR(KBr) ν_{max} 1729, 1741, and 1752 cm^{-1}; UV (EtOH) λ_{max} 277 ($\log\varepsilon$=3.14), and 285 nm (3.26). Found: C, 77.80; H, 5.95%. Calcd for $C_{26}H_{24}O_4$: C, 77.98; H, 6.04%.

Photoreaction of 3. A degassed solution of **3a–d** (1×10^{-5} M) in 2 ml of hexane was irradiated with a 100-W high-pressure Hg lamp through Pyrex filter and monitored by UV spectra and fluorescent spectra. Quantitative formation of the corresponding anthracene was confirmed for 5 min irradiation for all **3a—d**. However in the case **3a**, **b** which provide anthracenes **1a** and **b**, UV-absorption for the anthracenes gradually diminishes due to the formation of the corresponding known head to tall dimers.[19] In order to confirm the formation of benzene, irradiation of a nitrogen purged $CDCl_3$ (0.3 ml) solution of **1a**, **b**, **c**, and **d** (10 mg) in an NMR tube was performed. After 40 min irradiation with a 100 W high-pressure lamp, quantitative benzene formation was confirmed by the appearance of absorption band at δ=7.36 on each ^{1}H NMR spectrum.

Fluorescence Quantum Yields of 1 and 3. Fluorescence quantum yields of **1** and **3f** were determined in various solvents by the method of Berlman using 9,10-diphenylanthracene (Φ=0.83)[17] as reference.[6,16] The emission spectra of **3a—e** (2.5×10^{-4} M in hexane or a powder sample) were measured upon irradiation at 285 nm (excitation and emission slit width 3 nm) at room temperature by a Hitachi 228 spectrophotometer. To evaluate the fluorescence quantum yield from **3**, the area was compared to the area under the florescence curve for **3f** (Φ=1)[6] as reference which was collected at 285 nm with the same absorption number as that for **3**.

We thank the Okayama NMR center for the NMR spectra recorded on a Varian VXR-500 spectrometer and a Grant-in-Aid No.05453022 from the Ministry of Education, Science and Culture.

References

1) N. J. Turro, "Modern Molecular Photochemistry," Benjamin/Cummings, Menlo Park, CA (1978), pp. 608—609, and references therein.

2) a) M. Kimura, H. Okamoto, H. Kura, A. Okazaki, E. Nagayasu, K. Satake, S. Morosawa, M. Fukuzawa, M. Abdol-Halim, and D. O. Cowan, *J. Org. Chem.*, **53**, 3908 (1988); b) M. Kimura, H. Kura, K. Nukada, H. Okamoto, K. Satake, and S. Morosawa, *J. Chem. Soc., Perkin Trans. 1*, **1988**, 3307; c) N.C. Yang, M.-J. Chen, and P. Chem, *J. Am. Chem. Soc.*, **106**, 7310 (1984); d) N. C. Yang and X. Q. Yang, *J. Am. Chem. Soc.*, **109**, 3804 (1987); e) N. C. Yang and M. C. Horner, *Tetrahedron Lett.*, **1986**, 543.

3) Tables of anisotropic thermal parameters, atomic parameters of hydrogen atoms, bond lengths and angles involving hydrogen atoms, and structure factors have been deposited on Document No. 67047 at the Office of the Editor of Bull. Chem. Soc. Jpn.

4) C. K. Jhonson, "ORTEP II, Report ORNL-5138," Oak Ridge National Laboratory, Tennessee (1976).

5) a) D. A. Doughetry, W. D. Hounshell, H. B. Schlegel, R. A. Bell, and K. Mislow, *Tetrahedron Lett.*, **1976**, 3479; b) X. Zhou, R. Liu, and N. L. Allinger, *J. Am. Chem. Soc.*, **115**, 7525 (1993).

6) H. Okamoto, M. Kimura, K. Satake, and S. Morosawa, *Bull. Chem. Soc. Jpn.*, **66**, 2436 (1993).
7) a) E. S. Freeman and B. Carroll, *J. Phys. Chem.*, **62**, 394 (1958); b) H. L. Friedman, *J. Poly. Sci., Part C*, **C6**, 183 (1964).
8) D. Donati, G. Guarini, and P. Sarti-Fantoni, *Mol. Cryst. Liq. Cryst.*, **1972**, 187.
9) N. McDonald and C. E. Reineke, *J. Org. Chem.*, **32**, 1878 (1967).
10) H. H. Jaffe and M. Orchin, "Theory and Applications of Ultraviolet Specroscopy," Jhon Wiley and Sons, Inc., New York and London (1964), p. 584.
11) P. Main, G. Germain, and M. M. Woolfson, "MULTAN84, A System of Computer Programs for the Automatic Solution of Crystal Structures from X-Ray Diffraction Data," Univs. of York, England, and Louvain, Belgium (1984).
12) T. Ashida, "HBLSV. The Universal Crystallographic Computing System- Osaka," The Computation Center, Osaka Univ., Osaka (1973).
13) "International Tables for X-Ray Crystallography," Kynoch Press, Birmingham (Present distributor Kluwer Academic Publisher, Dordrecht) (1974), Vol. IV, pp. 22—98.
14) C. B. Warren and J. J. Broomfield, *J. Org. Chem.*, **38**, 4011 (1973).
15) P. G. Gassman and W. N. Shenk, *J. Org. Chem.*, **42**, 918 (1977).
16) I. B. Berlman, "Hand Book of Fluorescence Spectra of Atomic Molecules," Academic Press, New York and London (1965).
17) S. L. Murov, "Hand Book of Photochemistry," Marcel Dekker Inc., New York and London (1973), pp. 10 and 14.
18) a) W. Gerhartz, R. D. Poshuta, and J. Michl, *J. Am. Chem. Soc.*, **98**, 6427 (1976); b) R. B. Woodward and R. Hoffman, "The Conservation of Orbital Symmetry," Academic Press, New York (1970); c) R. A. Caldwell, *J. Am. Chem. Soc.*, **102**, (1980).
19) R. S-L. Shon, D. O. Cowan, and W. W. Schmiegel, *J. Am. Chem. Soc.*, **94**, 6779 (1972).